Journal of Applied Polymer Science

Effects of Cooling Temperature and Aging Treatment on the Morphology of Nano- and Micro-Porous Poly(ethylene-*co*-vinyl alcohol) Membranes by Thermal Induced Phase Separation Method

Hsu-Hsien Chang,[1] Konstantinos Beltsios,[2] Yih-Hang Chen,[1,3] Dar-Jong Lin,[1,3] Liao-Ping Cheng[1,3]

[1]Department of Chemical and Materials Engineering, Tamkang University, New Taipei city, 25137, Taiwan

[2]Department of Materials Science and Engineering, University of Ioannina, Ioannina, GR-45110, Greece

[3]Energy and Opto-Electronic Materials Research Center, Tamkang University, New Taipei city, 25137, Taiwan

Correspondence to: L.-P. Cheng (E-mail: lpcheng@mail.tku.edu.tw)

ABSTRACT: Poly(ethylene-*co*-vinyl alcohol) (EVOH 32) / 1,3-propanediol mixtures are processed by thermally induced phase separation for the formation of porous membranes. The crystallization line was determined both by the cloud-point and DSC methods. Two precursor solution compositions, four quench temperatures and various aging times were explored. It is found possible to generate both polymer-crystallization controlled morphologies (for high quenches and/or sufficiently aged dopes), especially globular microporous ones, and novel nano-scale porous morphologies dominated by intra-binodal phase separation (for low quenches and limited or no precursor solution aging). Structural characterization of the membranes was accomplished via application of scanning electron microscopy and wide angle X-ray diffraction. © 2014 Wiley Periodicals, Inc. J. Appl. Polym. Sci. **2014**, *131*, 40374.

KEYWORDS: membranes; crystallization; ageing; nanostructured polymers; morphology

Received 5 July 2013; accepted 30 December 2013

DOI: 10.1002/app.40374

INTRODUCTION

Poly(ethylene-*co*-vinyl alcohol) (EVOH) is a semicrystalline random copolymer commercially available mostly with a 27–47% mol ethylene content. EVOH copolymers of appropriate composition serve as optimized intermediates of hydrophobic polyethylene and overly hydrophilic (hence water/moisture sensitive) polyvinyl alcohol for various applications; certain EVOH products have attracted a great deal of attention in the biomedical field because they are blood compatible and wettable.[1] For example, hemodialysis by means of EVOH membranes has been investigated by Yamashita et al. with promising results.[2] Sakurada et al. used EVOH membrane to carry out efficient nonanticoagulant hemodialysis for renal failure patients.[3] In addition to biomedical applications, porous EVOH membranes are employed successfully in several other fields; e.g. as a microfiltration membranes in fine separation processes, as electrolyte separators in fuel cells, etc.,[4–8] because of the membranes' superior chemical resistivity and permeability.

One convenient method for producing symmetric porous membranes is through the so-called thermal induced phase separation (TIPS) process.[9–18] In this process, also describable as thermal phase inversion, a homogeneous polymer solution formed at an elevated temperature is rapidly cooled to a lower temperature; during the quench, one or more two-phase regimes are crossed and phase separation processes lead to the formation of networks of solid and low-viscosity liquid domains. Subsequent removal of the separated liquid phase gives rise to a continuous polymer matrix with statistically evenly distributed pores along the membrane thickness (*at least* when a symmetric structure is concerned, which is the usual case for ordinary TIPS). In a typical TIPS process, a third component acting as a nonsolvent is not a necessity, as the diluent itself ceases to support a *single* phase solution at the quenching temperature. Phase separation is induced either when the diluent turns into a *bad* solvent (in terms of the Flory-Huggins chi parameter, χ, which, as the temperature drops, increases and leads to the appearance of a binodal) or when a liquidus is crossed (this is an additional cause of solution phase separation in the case of crystallizable polymers). The nonnecessity of a third component, usually employable in the form of a nonsolvent bath, is an advantage of the TIPS method, compared to the quasi-alternative, nonsolvent induced phase separation (also known as 'immersion precipitation' or 'wet phase inversion') method, for which the maintenance of a fixed bath composition, necessary for a reproducible structural outcome, is always a difficult task.

EVOH membranes prepared by the TIPS process have been extensively studied by Matsuyama and Shang et al.[1,19–24] Various porous structures, stemming both from solid–liquid (S–L)

phase separation (i.e., polymer crystallization) and/or liquid–liquid (L–L) phase separation mechanisms, were obtained by changing the preparation conditions, such as polymer concentration, ethylene content of EVOH, cooling rate, solvent type, etc. For example, for the EVOH-glycerol binary system, membranes prepared from EVOH with high ethylene contents (e.g., 38%) often exhibited a cellular morphology; yet, those with low ethylene contents (e.g., 27%) tend to give particulate morphology. This is undoubtedly associated with the phase behavior of these systems. For the EVOH(38)-glycerol case, there exists a monotectic point at a 42 wt % EVOH content; at lower polymer contents a binodal dome emerges and the liquidus becomes metastable. On the other hand, for the EVOH(27)-glycerol case, only crystallization is experimentally observed, and a submerged binodal is expected. In addition, phase diagrams of mixtures of EVOH and poly(ethylene glycol) (PEG) have been determined.[25] Both the L-L phase separation and the crystallization boundaries were found to shift to higher temperatures for EVOH with higher vinyl alcohol content. However, the membrane structure was not reported in this EVOH/PEG system.

In the current research, we investigate key and novel aspects of TIPS fabrication of porous membranes from the 1,3-propanediol/EVOH binary pair; mixtures of the latter type are frequently described as 'dope' (i.e. viscous solution) in the literature of polymer membrane fabrication via various versions of phase inversion (wet phase inversion for flat membranes, wet spinning of hollow fiber membranes, thermal phase inversion for flat membranes etc). Special attention has been paid to the effect of the cooling scheme, particularly the quenching depth, and the dope ageing process. The latter process is of considerable interest, as it affects substantially the membrane morphology; yet ageing as a potentially important membrane morphology affecting factor is hardly ever mentioned in the TIPS literature. We have found that, by manipulating the cooling scheme alone, it is possible to affect the identity of the dominant morphology-determining phase separation process; morphologies dominated by either L-L phase separation or crystallization events could be obtained. For example, we have found that it is possible to generate lacy-type bi-continuous morphology (derived from spinodal decomposition) in addition to the crystallization-dominated particulate morphology obtained by Matsuyama et al.[1,23,24] from the same system. Under certain conditions, the obtained bi-continuous membranes exhibit a pore size in the 50–150 nm range. While we are aware of nanoporous polymeric membranes that have been prepared by self-assembly or template-etching methods,[26–28] we believe that this is the first time that symmetric bi-continuous membranes with such a low pore-size scale (50–150 nm) are obtained by either thermal or wet phase inversion process. The membrane preparation details and the effects of the preparation parameters, cooling scheme and polymer concentration, on the membrane morphology are discussed in the sections that follow.

METHODS

Material

Poly(vinyl alcohol-co-ethylene) (EVOH 32, a copolymer with a 32% ethylene mole content and M_n = 21,500 g/mole) was purchased from Aldrich. 1,3-propanediol was used as the diluent (latent solvent) for EVOH. All materials were used as received.

Phase Diagram Determination

The gelation (crystallization) phase boundaries for the binary system 1,3-propanediol/EVOH were determined by the cloud point method.[1,22–24] A specific amount of polymer (dried in an oven at 60°C) was mixed with the diluent and sealed in a glass bottle with a Teflon-lined cap. The mixture was blended on a roller at 130°C until the polymer was completely dissolved. This solution was then put in a thermostatically controlled oven maintained at a constant temperature for 14 days. The gelation points were identified as the compositions at which homogeneous solutions began to gel.

For comparison with the above gelation data, the melting and crystallization points for various precursor mixtures were determined by differential scanning calorimeter (MDSC 2920, TA Instrument Ltd., DE, USA). The sample was prepared by weighing the polymer and the solvent (typically 10–15 mg) into an aluminum liquid pan. The samples were heated to 200°C at a rate of 10°C/min, kept at this temperature for 1min, and then cooled to room temperature at the same rate. The onset of the exothermic peak during cooling was taken as the dynamic crystallization temperature.

Membrane Preparation and Characterization

EVOH membranes were prepared in the form of a flat sheet by the TIPS method. First, polymer was dissolved in 1,3-propanediol at 130°C on a roller to form a 20 or 30 wt % homogeneous solution. The solution was cooled and, before it gelled, placed in the cell for subsequent quenching experiments. As shown in Figure 1, the cell consists of two stainless steel plates (~2 mm thick) and a Teflon sheet (200 μm thick) having a square opening in the center. The Teflon sheet was sandwiched between the stainless steel plates to give a space of constant height. The sample was again heated at 130°C in an oven for 30 min to ensure complete dissolution of the polymer gel. Subsequently the sample was immersed in an isothermal water bath (60°C, 45°C, 25°C, or 5°C) to induce phase separation. The nascent membrane was soaked in water, in which the diluent, 1,3-propanediol, was extracted from the obtained membrane. The wet membrane was freeze-dried and characterized by the following methods:

1. Morphologies of the membranes were observed using a field emission scanning electron microscope (FESEM, Leo 1530, Carl Zeiss, Oberkochen, Germany). A piece of membrane sample was vacuum-dried and then attached to a sample holder by conductive copper tapes. The cross section of the membrane was obtained by fracturing the membrane in liquid nitrogen. Silver paste was applied at the edges of the sample to enhance conductivity. Then, the sample was sputtered with a thin layer (~2 nm) of Pt–Pd alloy and observed under a low acceleration voltage, 2 kV, by means of an in-lens detector. The pore and particle sizes in the SEM photographs were measured based on the calibrated scale, as shown in Table I.

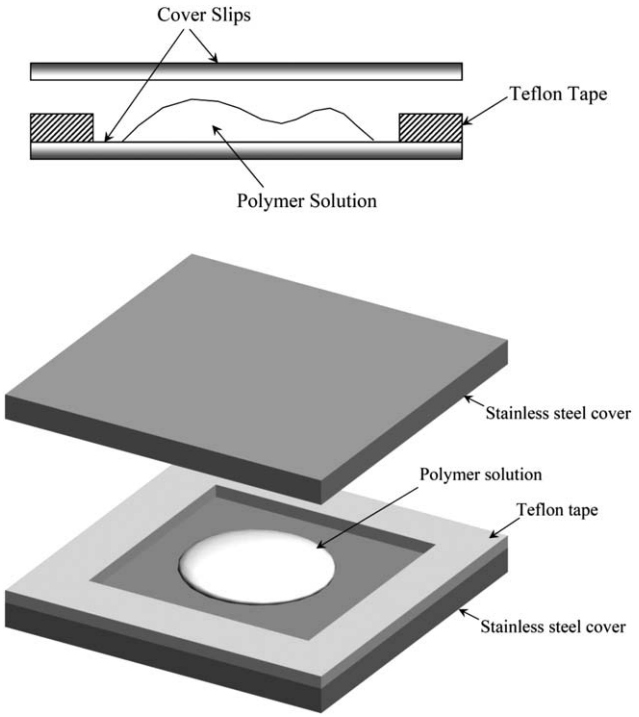

Figure 1. Schematic representation of the cell for membrane preparation.

2. The structure of EVOH crystals in the membrane was determined by a wide angle X-ray diffractometer (XRD, D8 Advance, Bruker, Karlsruhe, Germany). The operation parameters included: source intensity = 40 kV/40 mA, λ = 1.54 Å (copper K_α line), source slit width = 0.6 mm, increment = 0.05°/step, scanning speed = 3 s/step, and scanning range = $10° < 2\theta < 30°$. Crystallinity of the sample was determined by deconvolution of the diffraction peaks into amorphous and crystalline contributions, as shown in Table I, following a curving fitting method described in the literature.[29] The curve fitting scheme incorporated Gaussian and Lorenztian functions in a mixed form by means of a commercial software, GRAMS/AI™.

RESULTS AND DISCUSSION

Phase Diagram of the EVOH/1,3-Propanediol System

The phase diagram for the EVOH/1,3-propanediol system is shown in Figure 2. The filled squares (■) stand for the observed gelation

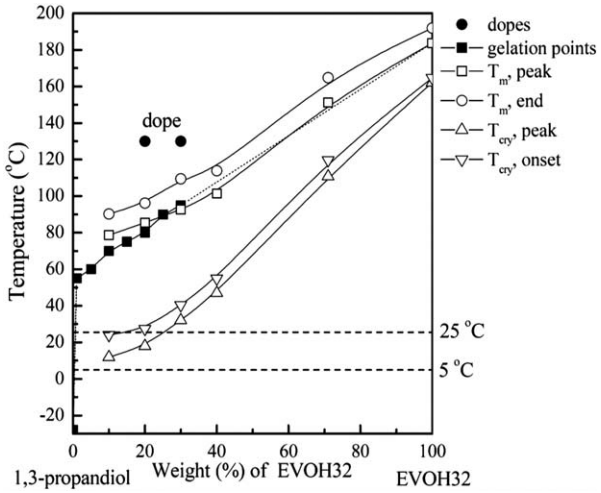

Figure 2. Phase diagram of the 1,3-propanediol/EVOH system. (a) Measured gelation points and DSC data; and (b) schematic binodal and spinodal drawn for the explanation of morphology formation.

points arising from S-L phase separation. Above these points there exists a one-phase region, in which homogeneous solutions can be prepared with long-term stability, whereas below these points, the prepared dopes would precipitate via crystallization into white gels. Because L-L phase separation was not observed over the studied composition range, the binodal and spinodal are assumed to be located below the gelation line; as the latter gelation is associated with crystallization the binodal is a "submerged" overall metastable one.

DSC has been used to determine the melting temperature and crystallization temperatures (cooling rate = 10°C/min) of the gels with different compositions. As shown in Figure 2(a), the temperatures of the gelation points are close to the DSC melting point (□, $T_{m,\ peak}$), yet they are much higher than the dynamic crystallization temperatures (T_{cry}). This is because the gelation points were determined after allowing the sample to approach phase equilibrium (upon standing for 14 days at a fixed temperature), while T_{cry} were obtained through a dynamic process. In the latter case, the value of T_{cry} depends on the dissolution state of the sample and the cooling rate for crystallization. For an initially well dissolved sample, T_{cry} increases with decreasing cooling rate because of a lower degree of super-cooling (overshooting). That is, a T_{cry} closer to the gelation point could be obtained by reducing the cooling rate of the DSC runs.

Table I. Preparation Conditions and Properties of EVOH Membranes

Dope (wt.%)	Cooling temperature (°C)	Dope reached time (min)[a]	Crystallinity[b] XRD (%)	Pores/particles size SEM (μm/nm)
20	60	~5	42.6 ± 1.2	Particles (1–2 μm)
	45	~4	43.1 ± 0.7	Particles (0.2–0.5 μm
	25	~2	42.8 ± 0.6	1–2 μm
	5	~1	41.9 ± 1.4	50–150 nm
30	45	~4	42.3 ± 0.4	Particles (0.5–1 μm)
	25	~2	42.8 ± 1.1	0.2–1 μm

[a] Micro-thermocouple measurement.
[b] Amorphous and crystalline regions being sorted by curve fitting technique.

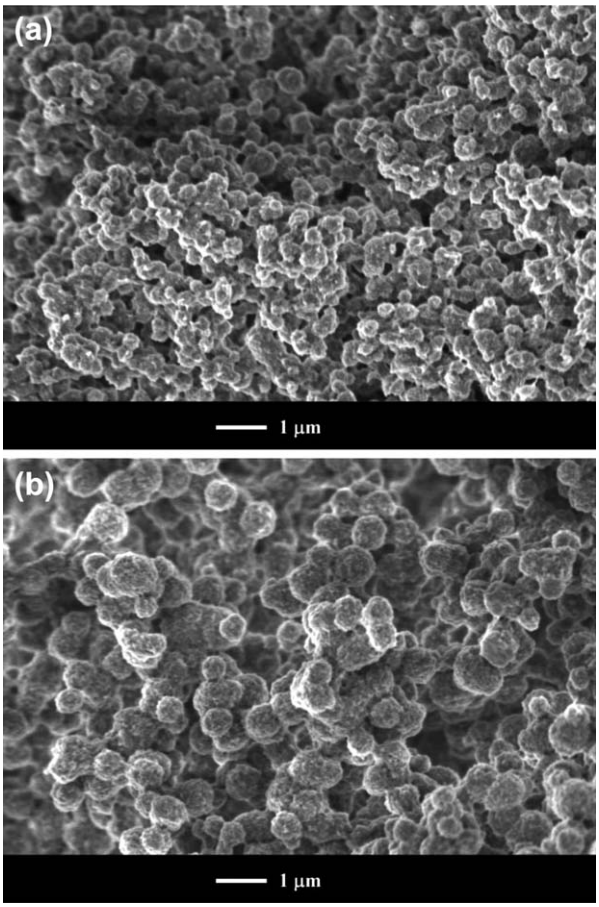

Figure 3. Cross-sectional morphologies of the EVOH membranes prepared by TIPS at 45°C. Polymer concentration in the dope: (a) 20 wt % and (b) 30 wt %.

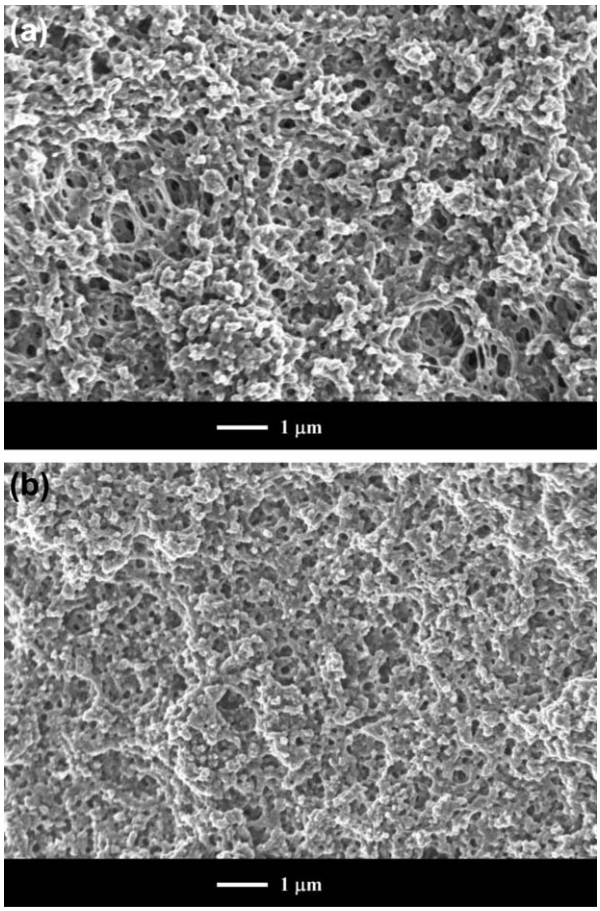

Figure 5. Cross-sectional morphologies of the EVOH membranes prepared by TIPS at 25°C. Polymer concentration in the dope: (a) 20 wt % and (b) 30 wt %.

Morphologies of EVOH Membranes Formed by TIPS

Effects of Cooling Bath Temperature and EVOH Concentration. The cross-sectional morphologies of the membranes formed at different quenching temperatures are shown in Figures 3–5. The starting mixture contains either 20% or 30% EVOH dissolved in 1,3-propandiol. In the case of quenching in 45°C bath, the formed membranes exhibit a particulate morphology for either dope composition, as shown in Figure 3. The latter type of morphology derives typically from polymer crystallization occurring in the dope that is brought into the crystallization zone.[23,24] The semi-crystalline particles have the shape of a sphere and form a network via interlinks; voids between particles form a network as well and, hence, the porosity is of the open type. As no *cellular* pores are observed in these membranes, it is possible that no liquid–liquid demixing, especially of the type of nucleation and growth of liquid micelles, has occurred at this quenching temperature and structure formation is controlled nearly exclusively by polymer crystallization; this has been argued repeatedly in the literature for related diluent/EVAL systems.[21–24] Yet, in principle, it is not impossible that the final structure bears some imprint from an addtional spinodal decomposition process; our group has provided a detailed model of such a situation for a three-component (polymer/solvent/nonsolvent) system.[30] The latter model can be applied here as well by simply assigning the role of the solvent/nonsolvent pair to the diluent plus quenching.

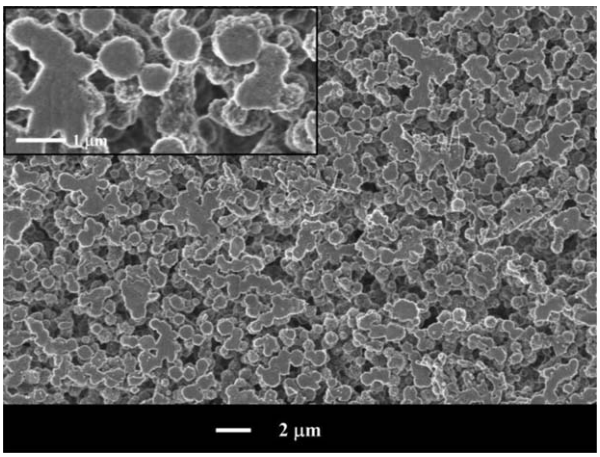

Figure 4. Surface morphology of the EVOH membrane prepared by quenching a 20 wt % dope to 45°C.

The comparison of Figure 3(a,b) suggests that higher polymer concentration gives rise to larger globules. This phenomenon has also been reported by Shang et al.[21,22] and Matsuyama

et al.,[23,24] and reflects a difference in nucleation density. Although one might expect that the larger temperature jump for the 30% precursor should favor nucleation more than the 20% precursor (ΔT for 30% and 20% precursor are 55°C and 70°C, respectively), it should not be overlooked that in the former case the precursor exhibits an enhanced viscosity. The viscosity effect is opposite to that of the temperature jump effect and, in the case of high quenches, it might well be the one that prevails. As is well known, a subcritical embryo may grow into a nucleus or re-dissolve in the solution; further growth requires that polymer chains can successfully deposit and rearrange on the embryo. In a very viscous dope, such as the 30% precursor, molecular motion becomes sluggish, and transportation of EVOH by solution diffusion to the embryo surface is not as effective as that for the 20% precursor. As the ΔT difference for the two dopes is only 15°C, the viscosity effect controls nucleation; polymer nucleates more sparingly in the more concentrated dope case and hence the corresponding membranes exhibit larger polymer domains. Morphology of the surface of the membranes bears close resemblance to that of the cross section. As shown in Figure 4, for the case of quenching the 20% dope to 45°C, some of the crystalline particles appear as truncated spheres with the flat sides deriving from growth against the stainless plate of the cell.

When the dopes (20% and 30% EVOH) were quenched into the 25°C bath, membranes with morphologies characteristic of L-L demixing of spinodal decomposition type were obtained, as shown in Figure 5. The pores and the polymer matrix intertwine into the lacy-like bi-continuous network evidencing prevalence of spinodal decomposition during the course of phase demixing. For the present binary system with submerged binodal and spinodal, both crystallization and L-L phase separation may occur depending on the details of quenching. If the bath temperature is higher than that for L-L demixing, cf. schematic binodal and spinodal in Figure 2(b), then crystallization is the only possible means for phase demixing, which corresponds to the case of quenching to 45°C shown in Figure 3. However, if the dope is quenched into the spinodal region (e.g. 25°C and 5°C in the present study), L-L demixing via spinodal decomposition (SD) would take place largely prior to crystallization and dominate the porous structural formation, based on the fact that SD is an essentially spontaneous process, whereas for crystallization there is an activation energy barrier to overcome. During SD separation and subsequent ripening of the SD-derived structure, crystallization may occur and eventually fix the microporous structure. Furthermore, DSC measurements show that it takes ~11 min for crystallization to commence at 25°C (cf. onset of crystallization), when the dope is cooled from 130°C at the rate of 10°C/min. For the present TIPS setup, the dope reached 25°C in ~2 min, according to microthermocouple temperature data (Table I). Therefore, SD is expected to take place first and lead to a lacy structure (often a characteristic SD outcome) before the nucleation of semicrystalline domains. Still the phases and/or compositions resulting from SD separation are not equilibrium ones and this is more generally true irrespectively of the exact intrabinodal (NG or SD) phase separation mode, when the latter prevails within a

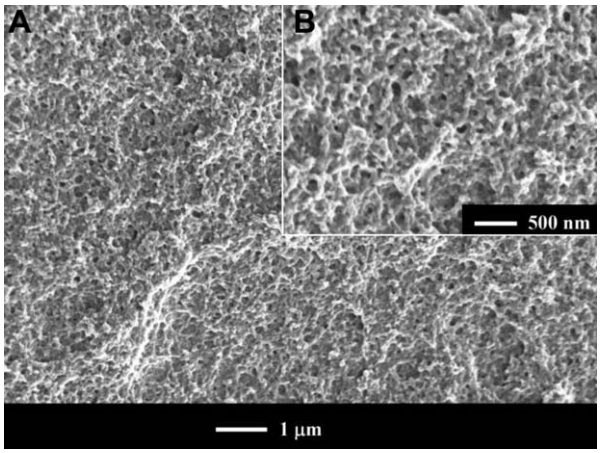

Figure 6. Cross-sectional morphologies of the EVOH membrane prepared by quenching a 20 wt % dope at 130°C to 5°C. (b) is the high magnification image of (a).

submerged miscibility gap. Consequently polymer crystallization is possible at a later stage; in our case the latter event leaves its mark in the form of a particulate polymer fine structure on the SD-derived lacy skeleton.

Comparison of Figures 5(a,b) reveals that the pore size decreases with increasing polymer concentration. A possible main reason for the latter trend is the following: if we simplify the situation by assuming that phase separation occurs when the quenching process approaches the spinodal, then for a higher polymer concentration the spinodal will be reached at a lower temperature (which will favor a smaller original phase separation wavelength and slower coarsening). We also note that some larger pores (1 μm range) are present as well; this is clearer in the case of the 20 wt % dope. Two families of pores can result from a two-stage L-L separation process.[31] At the same time it is of interest to find that the walls of the larger pores appear to have undergone deformation as lower density material was pulled between regions of more dense material; deformation possibly occurs during solidification and it is expected to be easier for a lower polymer fraction, hence for a higher-porosity, less-robust porous structure.

When the dope was quenched to 5°C, the pores of the formed membrane became very small, ca. 50–150 nm and, quite interestingly, they remained interconnected, as shown in Figure 6. In other words, the membrane appears as a mat consisting of two interwoven networks (a nano-porous network and a polymer framework) with a characteristic dimension at the nano-scale; a bi-continuous morphology at such a small length scale might be reported for the first time in the thermal/wet phase inversion membrane literature. Obviously, for a low quenching temperature, the dope ends up deeply into the spinodal region, cf., Figure 2. For a given overall composition, lower quenches are expected to give rise to smaller spacings.[32,33] The concentrated polymer-rich phase and the enhanced viscosity (even possibly a glass transition) inhibit the growth and coarsening of the amorphous phases resulting from spinodal decomposition. Consequently, the porous structure is fixed at an earlier stage, and small yet continuous main pores form. These findings show

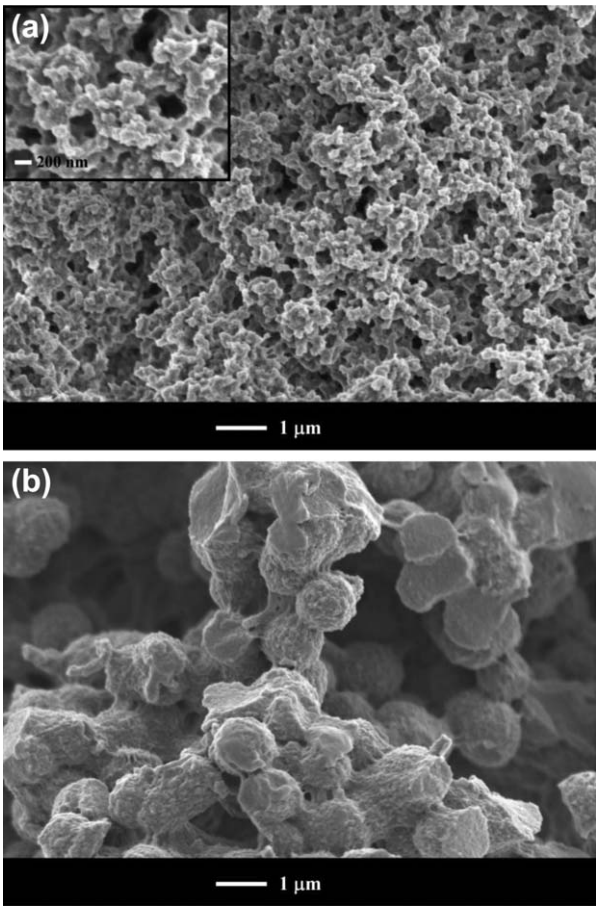

Figure 7. Cross-sectional morphologies of the EVOH membranes prepared by quenching the dope aged at 60°C for (a) 1 hr and (b) 2 hr. Temperature of the quenching bath is 25°C. EVOH concentration is 20 wt %.

that the membrane structure, including pore structure and pore size, can be manipulated by a precise control of the quenching temperature. In addition, on the basis of the microstructures presented in Figures 3, 5, and 6, it follows that in principle one might impose a thermal gradient along the thickness of the dope and attain an asymmetric membrane structure that exhibits nano-porosity at the top and porosity at the micron scale towards the bottom.

Effect of Precursor-Aging on the Membrane Morphology. In addition to the morphology control based on the quenching temperature, membrane morphology can be adjusted via aging of the dope below the gelation temperature for a certain period of time before quenching. While the availability of dope aging as an additional morphology-controlling parameter tends to be overlooked in the TIPS literature, the morphological effect through proper tuning of the aging process can be, at least in some cases, a quite remarkable one. It is also pertinent to note that a strong aging effect is possible in the case of *wet* phase inversion of semicrystalline polymers, as it has been demonstrated previously by us.[34] For the cases of aging the dope at 60°C for 1 and 2 hr prior to quenching in a 25°C bath, the formed membranes exhibit two very different morphologies, as shown in Figure 7. Aging for 1 hr gives rise to a lacy skeleton similar to that of a corresponding membrane prepared without aging (c.f. Figure 5); however, this membrane exhibited a more pronounced particulate microstructure. In contrast, when the same dope was aged for 2 hr before quenching, a morphology dictated by polymer crystallization was produced. The membrane structure consists of globular entities of ca. 1 μm with little evidence for a spinodal decomposition process. Through aging the dope at 60°C, a point sufficiently below the gelation line yet above the binodal, polymer nuclei or prenucleation embryos are expected to form without the interference of L-L demixing. Upon quenching this incipient dope to 25°C, it is possible that polymer crystallization would override L-L separation and dominate structural development, depending on the aging time (or equivalently on the level of crystalline domains/nuclei developed during aging). Apparently, during the 2-hr aging period crystal nuclei have grown to such an extent that polymer crystallization can compete effectively with L-L separation upon quenching to 25°C. On the other hand, when the dope was aged only for 1 hr, the formed nuclei might have been few; hence, after the dope was quenched, spinodal decomposition took place first to produce the lacy matrix, and then crystallization followed on the soft gel-phase to generate aggregated small particles, 100–200 nm; more precisely most of the latter particles result from crystallization following SD but some might correspond to small nuclei that have formed during the limited (1 hr long) aging. Spinodal decomposition can proceed without being affected by a dispersion of a limited number of crystalline nuclei; the latter will be engulfed by the structure that will result from SD, and/or they might serve as nuclei for the subsequent polymer crystallization. It might also be noted that if crystallization during aging is extensive, a substantial horizontal shift of the composition of the solution that undergoes further phase separation is also possible. For example the solution composition might shift from outside the binodal to the metastable regime of the binodal or to the spinodal regime or to the critical regime. However, as the compositional shift becomes stronger as the original crystallization becomes more extensive the pertinent morphological consequences might, overall, often be one of the secondary significance. Then for quenches to the right of the binodal the consequences might well be stronger for the less concentrated dopes. Finally if there is a feature related to spinodal decomposition in Figure 7(b) that might be a superimposed coarsened SD structure at the scale of few micrometers; at the latter scale areas rich in globules appear to alternate with areas free of matter.

The depth of quench also affects the membrane morphology considerably, even for aged dopes; this is illustrated in Figure 8. The dope aged at 60°C for 2 hr was immersed in the 5°C bath (i.e. a low quench). Unlike the crystallization-dominant morphology shown in Figure 7(b) (25°C bath), this membrane exhibits a bi-continuous lacy structure again. This suggests that spinodal decomposition has occurred extremely fast and dictated the phase demixing process in this low quench case, even though there might exist substantial amount of crystalline nuclei in the original dope. However, polymer crystallization did follow spinodal decomposition and left its imprint in the form of crystalline particles on the pore wall, as shown in the

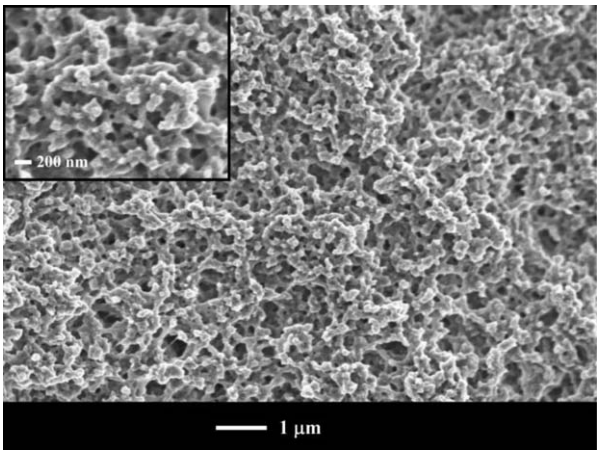

Figure 8. Cross-sectional morphology of the EVOH membrane prepared by quenching the dope aged at 60°C for 2 hr. Temperature of the quenching bath is 5°C. EVOH concentration is 20 wt %.

inset of Figure 8. X-ray diffraction data given in a subsequent section (XRD Analyses of the Membranes) support this morphological observation. It is interesting to note that the pore size of this membrane is about 1–2 μm, i.e. significantly larger than the nanopores shown in Figure 6 for the same quenching temperature, but without going through the dope-aging procedure. This may be explained as follows. When nuclei or small crystalline entities were generated during aging, pure liquid solvent was rejected simultaneously to the vicinity of the crystallites. These liquids dilute the EVOH solution surrounding the crystallites, which upon quenching, gives rise to a more porous morphology.

Upon dope aging at 80°C for 2 hr, and subsequent immersion into a 25°C bath, a morphology characteristic of spinodal decomposition is observed (Figure 9); the latter resembles the one obtainable without aging [c.f. Figure 5(a)]. As the gelation point is close to 80°C for this precursor solution composition (c.f. Figure 2), aging to form nuclei is not effective in this case (in general, it takes a few days for this particular dope to become gel exhibiting crystallinity). As a result, even after a 2-hr aging process, spinodal decomposition dictates the phase separation process and a bicontinuous lacy-structure results.

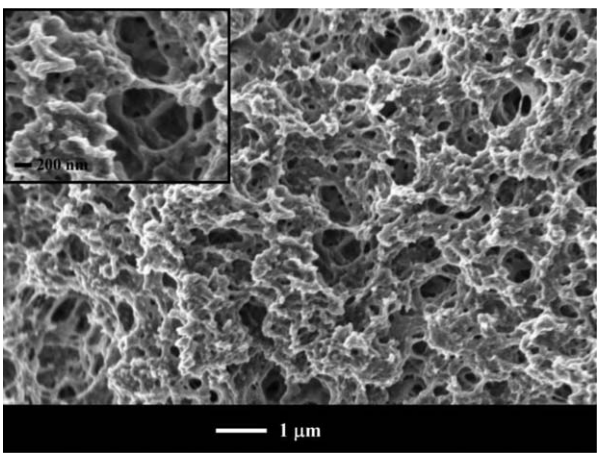

Figure 9. Cross-sectional morphology of the EVOH membrane prepared by quenching the dope aged at 80°C for 2 hr. Temperature of the quenching bath is 25°C. EVOH concentration is 20 wt %.

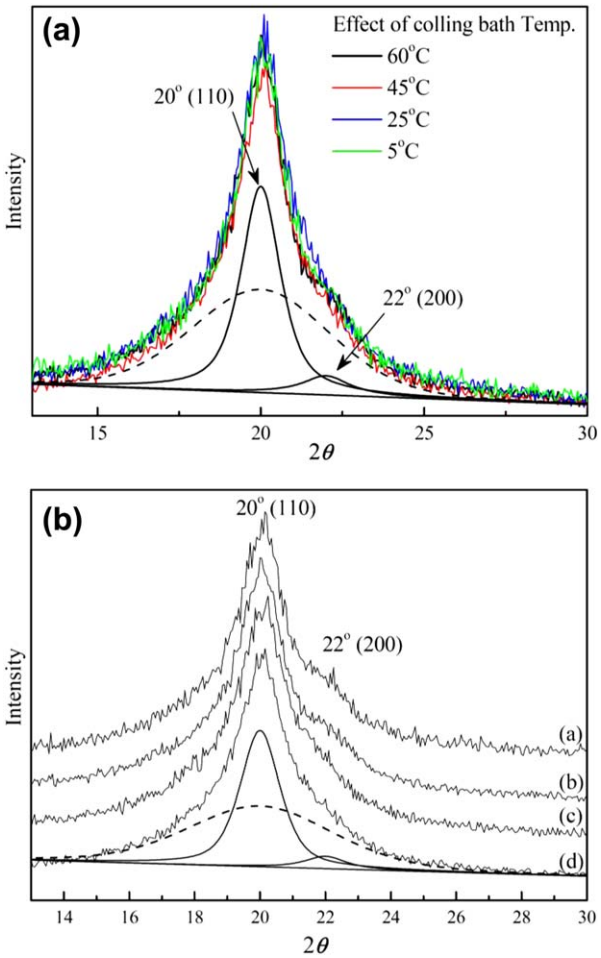

Figure 10. XRD diffractograms of EVOH membranes prepared under different conditions. (a) EVOH concentration = 20 wt %, bath temperature = 5°C, 25°C, 45°C, 60°C, amorphous and crystalline regions being sorted by curve fitting technique for the membrane quenched at 5°C; (b) Curves a: 20 wt % EVOH, 45°C bath, b: 30 wt % EVOH, 45°C bath, c: 20 wt % EVOH, 25°C bath, d: 30 wt % EVOH, 25°C bath. [Color figure can be viewed in the online issue, which is available at wileyonlinelibrary.com.]

XRD Analyses of the Membranes

The crystal structures of various membranes were determined by XRD analysis. As shown in Figure 10, the diffraction patterns of all prepared membranes are similar. The diffraction peaks at 20.0° and 22.0° correspond to the reflection of (110) and (200) planes, typical for the EVOH32 in its crystalline phase.[35–37] The diffraction patterns could be decomposed into amorphous (a broad amorphous area around 2θ = 20.0°) and crystalline contributions by a curve fitting technique. As an example, the decomposed patterns of the membrane M50 are shown in Figure 10(a), from which the crystallinity was calculated to be 43%.[38,39] The crystallinities of other membranes were determined in the same manner (Table I). It is of interest that the crystallinity levels for all formed membranes are close to each other, irrespectively of EVOH content in the dope or at different

cooling baths. This implies that although crystallization may occur at different stages of the TIPS process and yield membranes with different morphologies, for the present system, the crystallinity level appears to be a largely inherent feature of the particular (as regards composition and molecular weight) polymer, at least when solidified from concentrated solution, while the contribution of the choice of parameters such as aging time and quenching temperature is, within limits, only a weak one.

CONCLUSIONS

From the study of the 1,3-propanediol/EVOH phase diagram and the morphologies of the membranes formed via versions of the TIPS process the following conclusions can be drawn:

1. The moderate proximity of the polymer liquidus and the submerged binodal allow for widely different membrane structures in the case of TIPS processing of 1,3-propanediol/EVOH dopes, while aging of the precursor solution offers additional structural options.
2. High quenches and/or sufficiently aged dopes lead to globular microporous membranes with crystallization processes dominating structure formation.
3. Low quenches and limited or no aging of the precursor solution lead to nanoporous membranes with morphology dominated by spinodal decomposition.

The authors thank the National Science Council of Taiwan for the financial support (NSC 96-2628-E-032-001-MY3).

REFERENCES

1. Shang, M. X.; Matsuyama, H.; Maki, T.; Teramoto, M.; Lloyd, D. R. *J. Appl. Polym. Sci.* **2003**, *87*, 853.
2. Yamashita, S.; Nagata, S.; Takakura, K. US Patent **1979**, 4,134,837.
3. Sakurada, Y.; Sueoka, A.; Kawahashi, M. *Polym. J.* **1987**, *19*, 501.
4. Zhang, Y. J.; Huang, Y. D.; Wang, L. *Solid State Ionics* **2006**, *177*, 65.
5. Lagaron, J. M.; Powell, A. K.; Bonner, G. *Polym. Test.* **2001**, *20*, 569.
6. Avramescu, M. E.; Sager, W. F. C.; Wessling, M. *J. Membrane Sci.* **2003**, *216*, 177.
7. Young, T. H.; Cheng, L. P.; Lin, H. Y. *Polymer* **2000**, *41*, 377.
8. Zhou, J.; Meng, S.; Guo, Z.; Du, Q. G.; Zhong, W. *J. Membrane Sci.* **2007**, *305*, 279.
9. Alwattari, A. A.; Lloyd, D. R. *J. Membrane Sci.* **1991**, *64*, 55.
10. Kim, S. S.; Lloyd, D. R. *J. Membrane Sci.* **1991**, *64*, 13.
11. Kim, S. S.; Lim, G. B. A.; Alwattari, A. A.; Wang, Y. F.; Lloyd, D. R. *J. Membrane Sci.* **1991**, *64*, 41.
12. Lim, G. B. A.; Kim, S. S.; Ye, Q. H.; Wang, Y. F.; Lloyd, D. R. *J. Membrane Sci.* **1991**, *64*, 31.
13. Lloyd, D. R.; Kim, S. S.; Kinzer, K. E. *J. Membrane Sci.* **1991**, *64*, 1.
14. Lloyd, D. R.; Kinzer, K. E.; Tseng, H. S. *J. Membrane Sci.* **1990**, *52*, 239.
15. Vanegas, M. E.; Quijada, R.; Serafini, D. *Polymer* **2009**, *50*, 2081.
16. Okada, K.; Nandi, M.; Maruyama, J.; Oka, T.; Tsujimoto, T.; Kondoh, K.; et al. *Chem. Commun.* **2011**, *47*, 7422.
17. Shen, Y.; Qi, L.; Mao, L. Q. *Polymer* **2012**, *53*, 4128.
18. California, A.; Cardoso, V. F.; Costa, C. M.; Sencadas, V.; Botelho, G.; Gomez-Ribelles, J. L.; et al. *Eur. Polym. J.* **2011**, *47*, 2442.
19. Fu, S. S.; Matsuyama, H.; Teramoto, M.; Lloyd, D. R. *J. Chem. Eng. Jpn.* **2003**, *36*, 1397.
20. Shang, M. X.; Matsuyama, H.; Teramoto, M.; Lloyd, D. R.; Kubota, N. *Polymer* **2003**, *44*, 7441.
21. Shan, M. X.; Matsuyama, H.; Teramoto, M.; Okuno, J.; Lloyd, D. R.; Kubota, N. *J. Appl. Polym. Sci.* **2005**, *95*, 219.
22. Shang, M. X.; Matsuyama, H.; Maki, T.; Teramoto, M.; Lloyd, D. R. *J. Polym. Sci. Polym Phys.* **2003**, *41*, 194.
23. Matsuyama, H.; Iwatani, T.; Kitamura, Y.; Tearamoto, M.; Sugoh, N. *J. Appl. Polym. Sci.* **2001**, *79*, 2449.
24. Matsuyama, H.; Iwatani, T.; Kitamura, Y.; Tearamoto, M.; Sugoh, N. *J. Appl. Polym. Sci.* **2001**, *79*, 2456.
25. Liu, B.; Du, Q. G.; Yang, Y. L. *J. Membrane Sci.* **2000**, *180*, 81.
26. Newton, M. R.; Bohaty, A. K.; White, H. S.; Zharov, I. *J. Am. Chem. Soc.* **2005**, *127*, 7268.
27. Olson, D. A.; Chen, L.; Hillmyer, M. A. *Chem. Mater.* **2008**, *20*, 869.
28. Liu, N. G.; Dunphy, D. R.; Atanassov, P.; Bunge, S. D.; Chen, Z.; Lopez, G. P.; et al. *Nano Lett.* **2004**, *4*, 551.
29. Lin, D. J.; Chang, H. H.; Chen, T. C.; Lee, Y. C.; Cheng, L. P. *Eur. Polym. J.* **2006**, *42*, 1581.
30. Lin, D. J.; Beltsios, K.; Chang, C. L.; Cheng, L. P. *J. Polym. Sci. Polym. Phys.* **2003**, *41*, 1578.
31. Beltsios, K.; Athanasiou, E.; Aidinis, C.; Kanellopoulos, N. *J. Macromol. Sci. Phys.* **1999**, *B38*, 1.
32. Beltsios, K. G.; Bedard, M. C. M. *J. Macromol. Sci. Phys.* **2000**, *B39*, 623.
33. Huston, E. L.; Cahn, J. W.; Hilliard, J. E. *Acta Metall. Mater.* **1966**, *14*, 1053.
34. Lin, D. J.; Beltsios, K.; Young, T. H.; Jeng, Y. S.; Cheng, L. P. *J. Membrane Sci.* **2006**, *274*, 64.
35. Lopez-Rubio, A.; Lagaron, J. M.; Gimenez, E.; Cava, D.; Hernandez-Munoz, P.; Yamamoto, T.; et al. *Macromolecules* **2003**, *36*, 9467.
36. Huang, C. H.; Wu, H. M.; Chen, C. C.; Wang, C. W.; Kuo, P. L. *J. Membrane Sci.* **2010**, *353*, 1.
37. Cerrada, M. L.; Perez, E.; Perena, J. M.; Benavente, R. *Macromolecules* **1998**, *31*, 2559.
38. de Lima, J. A.; Felisberti, M. I. *Eur. Polym. J.* **2008**, *44*, 1140.
39. Russo, P.; Acierno, D.; Di Maio, L.; Demma, G. *Eur. Polym. J.* **1999**, *35*, 1261.